Bonding and compressibility in molecular and polymeric phases of solid CO_2

2004 J. Phys.: Condens. Matter 16 S1263

(http://iopscience.iop.org/0953-8984/16/14/038)

INSTITUTE OF PHYSICS PUBLISHING JOURNAL OF PHYSICS: CONDENSED MATTER

J. Phys.: Condens. Matter **16** (2004) S1263–S1270 PII: S0953-8984(04)75042-0

Bonding and compressibility in molecular and polymeric phases of solid CO_2

L Gracia[1], M Marqués[2], A Beltrán[1], A Martín Pendás[2] and J M Recio[2]

[1] Departament de Ciències Experimentals, Universitat Jaume I, E-12080 Castelló, Spain
[2] Departamento de Química Física y Analítica, Universidad de Oviedo, E-33006 Oviedo, Spain

E-mail: mateo@fluor.quimica.uniovi.es (J M Recio)

Received 22 January 2004
Published 26 March 2004
Online at stacks.iop.org/JPhysCM/16/S1263
DOI: 10.1088/0953-8984/16/14/038

Abstract

We present the results of a theoretical study of the response of molecular CO_2-I and CO_2-III, and polymeric CO_2-V polymorphs to hydrostatic pressure. Total energy calculations and geometry optimizations have been performed under the local density functional approximation combining a pseudopotential and planewave scheme as implemented in the VASP code. Using the atoms in molecules theory, the network of inter- and intra-molecular chemical bonds of the different phases are rigorously characterized in terms of the values of the electron density and the Laplacian at the bond critical points. The chemical graph of a hypothetical orthorhombic structure displays bonding features that are associated with a precursor geometry of polymeric carbon four-fold coordinated phases. In addition, the bulk compressibility is decomposed into atomic and molecular contributions with the aim of providing a better understanding of the reasons that explain the emergence of low compressible polymorphs at high pressures.

1. Introduction

Empirical correlations involving nearest neighbour distances, vibrational frequencies, and bulk moduli suggest that high-pressure polymeric polymorphs of CO_2 can exhibit hardness comparable or superior to diamond. This fact has given rise to a great interest with much effort directed to the description of the progressive transformations of solid CO_2 under hydrostatic pressure (p). In the last decade, a considerable amount of theoretical and experimental data was collected for structural and phase transition properties of two molecular (CO_2-I and CO_2-III) [1–6] and one polymeric (CO_2-V) phases [7–13]. More recently, several experimental papers inform of the appearance of new pseudo-molecular polymorphs (CO_2-II and CO_2-IV) after heating CO_2-III [14–16]. In addition, CO_2 is found to decompose *via* the formation of a new CO_2-VI phase at $p > 40$ GPa and temperatures lower than expected from theory and experiments [17].

Some of the reported information is the subject of current debate. Thus, assuming the equilibrium geometry of the CO_2 molecule, the analysis of x-ray diffraction data found $a < b < c$ for the $Cmca$ structure of CO_2-III [3], whereas recent calculations predicted $b < a < c$ without explicit values for the intramolecular C–O distances [6, 8]. High-pressure experimental investigations also found a not entirely molecular behaviour for CO_2-III, with intermolecular interactions that might be incompatible with the presence of gas-like CO_2 units in its lattice, and suggest this phase as a precursor for polymeric CO_2-V [9, 14]. Moreover, the experiments first proposed an α-quartz-type structure [7] and later a tridymite-type lattice for CO_2-V with a zero pressure bulk modulus (B_0) as high as 365 GPa [9]. First-principles calculations based on density functional theory concluded that 'a β-cristobalite-like phase is energetically the favoured polymeric CO_2 phase' [11] and that B_0 in this and the experimental proposed structures is around only 150 GPa [12].

It is to be remarked that thermal effects have to be considered in the discussion and the comparison between the experimental and the theoretical information. Specifically, temperature (T) plays an important role at least in three basic aspects:

(i) the modification of structural and equation of state (EOS) parameters of the molecular phases, which is already important at room T, and is clearly much greater than in the extended solids;
(ii) the localization of thermodynamic phase boundaries since T may affect in a substantial different manner the free energy of the several phases; and
(iii) the determination of the phase transition hysteresis ranges due to the different kinetic barriers involved in molecular–molecular and molecular–polymeric transformations.

With all these considerations in mind, we have started a theoretical investigation aimed at contributing to the understanding of several of the unresolved questions related to the polymorphic sequence of solid CO_2. Our concerns in this contribution are focused on some of the observed changes in the structural, electronic, and elastic properties of CO_2-I, CO_2-III, and CO_2-V. In particular, the chemical bonding of the polymorphs considered for the three phases is rigorously characterized by means of the atoms in molecules (AIM) theory [18, 19]. Within this formalism, the identification and the chemical nature of intra- and inter-molecular interactions can be determined. Moreover, the atomic contributions to the bulk compressibility of all the structures are evaluated. This analysis allows us to provide information on the potential super-hard behaviour of the high-pressure CO_2 polymorphs.

2. Computational aspects

2.1. Total energy calculations and EOS determination

First-principles total energy (E) calculations were carried out within the density-functional theory framework using a plane-wave pseudopotential scheme, as implemented in the Vienna *ab initio* simulation package (VASP) [20]. We used the Ceperley–Alder local density exchange–correlation functional [21] and the projector augmented wave all-electron description of the electron–ion-core interaction [22]. This rather standard scheme allows highly accurate calculations to be achieved with a low-energy cutoff. In addition, the Brillouin zones have been sampled through Monkhorst–Pack k-space grids that assure energetic convergence for all the crystal structures considered in this work.

The calculations have been performed in the cubic ($Pa\bar{3}$) and orthorhombic ($Cmca$) lattices of CO_2-I and CO_2-III, respectively, whereas for the polymeric CO_2-V phase we have considered the β-cristobalite ($I\bar{4}2d$), tridymite ($P2_12_12_1$), and stishovite

($P4_2/mnm$) crystal structures. At selected values of the molecular volume (V), we have optimized the lattice parameters (a, b, c) and the atomic coordinates of the corresponding unit cells by requiring zero forces acting on the carbon and oxygen atoms. For the stishovite structure this procedure yields a repulsive E–V curve that presents an equilibrium geometry only if the c/a ratio is kept fixed. (E, V) computed points have been described with numerical and analytical functions to provide EOS parameters and the equilibrium unit cell configuration as a function of pressure for all the phases considered. These tasks are carried out with our code GIBBS [23] that includes also a quasi-harmonic Debye model to deal with temperature effects [24].

2.2. Topological analysis of the electron density

The topology of the electron densities coming from all-electron crystalline wavefunctions derived with the CRYSTAL package [25] at the VASP optimized geometries is investigated using the AIM theory [18]. In this formalism, the electron density critical points have a full chemical meaning. Global maxima of the electron density usually correspond to the nuclei positions of the crystal, whereas a first-order saddle critical point identifies a bond point and provides an unequivocal criterion to establish when two atoms are bonded. Bond points have one-dimensional repulsion basins that define the bond paths. The position of the bond critical point along the bond path, the value of the electron density (ρ_b) and the Laplacian ($\nabla^2\rho_b$) at that point inform on the strength and the nature of the chemical bond between the two atoms.

For our purposes, one of the most important aspects of this theory is that the unit cell volume can be divided into non-overlapping atomic regions containing one nucleus and surrounded by surfaces where the local flux of the electron density gradient is nil. Appropriate integrations within these basins yield atomic volumes (V_i) and charges ($\mathcal{Q}_i$), and if we add the atomic volumes of the atoms contained in the unit cell then we recover the unit cell volume. The localization of the critical points of the electron density, the determination of the atomic basins, and the evaluation of V_i and $\mathcal{Q}_i$ are performed by means of a computational program called CRITIC [26].

3. Results and discussion

3.1. Structure and equations of state

The most interesting results from our structural optimizations in CO_2-I, CO_2-III, and CO_2-V phases are collected in table 1. For CO_2-III, we include the geometry of a zero pressure unit cell ($Cmca(2)$) extrapolated from the high-pressure experimental data reported by Aoki *et al* [3]. $Cmca(2)$ has intra-molecular C–O distances ($d_{C–O}$) 0.1 Å greater than $Cmca(1)$, the latter keeping the geometry of the gas phase CO_2 molecule, as in the cubic $Pa\bar{3}$ phase. Next nearest neighbours distances ($d^{nn}_{C–O}$) are also similar, but correlate in a different way with the T-like (T) and slipped parallel (P) dimeric configurations present in CO_2-III. Distances between oxygens ($d_{O–O}$) are again similar in $Cmca(1)$ and $Pa\bar{3}$ and slightly shorter than in $Cmca(2)$. It is to be emphasized that the order of the calculated lattice parameters in $Cmca(1)$ coincides with that found in recent calculations [6, 8]. As a general result, the shortest C–O distances increase and O–O distances decrease in passing from the molecular to the polymeric structures, and in the latter as the coordination index increases. The same behaviour is found for B_0, whereas the zero pressure volume (V_0) shows the opposite trend.

As regards the comparison with available experimental data, thermal effects at 296 K increase a in CO_2-I to 5.726 Å (5.827 Å in the experiments [27]) and decrease B_0 to 2.8 GPa

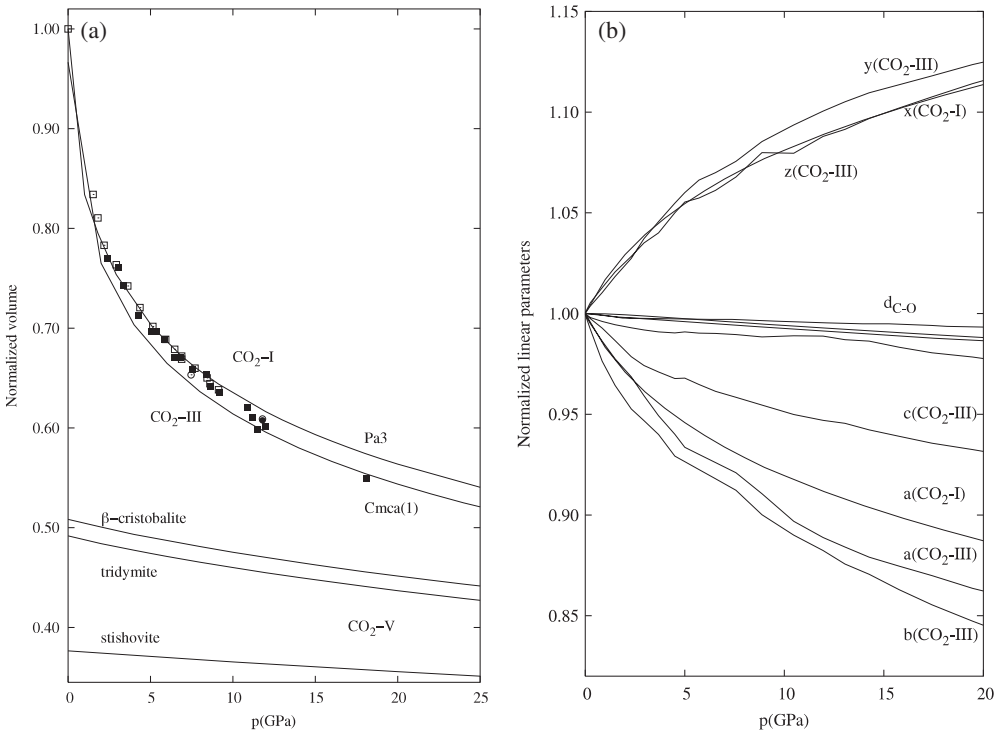

Figure 1. Calculated room temperature normalized volume (a) and static normalized linear parameters (b) *versus* pressure for CO_2-I, CO_2-III, and CO_2-V phases. Open symbols (squares [27], circle [3]) and solid symbols (squares [28], circle [3]) stand for the experimental data in CO_2-I and CO_2-III, respectively, at room temperature. Curves under the $d_{C–O}$ label include results from polymeric phases.

(2.9 GPa in the experiments [28]). Furthermore, the $V/V_0–p$ diagram (V_0 is the corresponding zero pressure volume of the CO_2-I phase) depicted in figure 1 shows a very good agreement between the calculated and the experimental data at similar temperatures. We found the CO_2-I $\rightarrow$ CO_2-III transition around 17 GPa with a negligible volume reduction, also in concordance with the experimental observations [3, 29]. Contrarily to the low compressible tridymite phase proposed in the x-ray measurements of Yoo *et al* [9], we found β-cristobalite as the lowest energy structure at zero pressure with a B_0 value of 142.7 GPa (see also [11] and [12]). It is to be noted that a high B_0 value close to 330 GPa is predicted only in the hypothetical strained stishovite structure.

The analysis of the pressure effects on the linear parameters of the molecular phases shows that the lattice parameter reduction is roughly compensated by the increase of the oxygen internal coordinates resulting in a nearly constant dependence of the intramolecular C–O distance with pressure. This is the expected behaviour for a molecular solid. Interestingly enough, we observe that a similar trend is found for $d_{C–O}$ in the polymeric phases (see figure 1). It may be concluded that the lower compressibility of these phases is related to the increase in the coordination index while the difficulty to approach C and O atoms remains about the same in the two types of solids (molecular and non-molecular). Thus, pressure brings CO_2 molecules near to each other in the molecular phases while rotates CO_4 tetrahedra in the four-fold coordinated structures. As the O–C–O angles are difficult to change, the compressibility of the polymeric phase decreases.

Table 1. Zero pressure cell parameters (Å), formula unit volumes (Å^3), bulk moduli (GPa) and selected bond distances (Å) of CO_2-I ($Pa\bar{3}$), CO_2-III ($Cmca(1)$ and $Cmca(2)$), and CO_2-V ($P2_12_12_1$, $I\bar{4}2d$, and $P4_2/mnm$) polymorphs according to our static calculations. Z stands for the number of molecules in the unit cell, the subscript nn means next nearest neighbours, numbers in brackets refer to the multiplicity of the bond, and T and P designate, respectively, the T-like and parallel configurations of two CO_2 units in the molecular CO_2-III phase. The second row of $d_{O–O}$ contains average distances between the number of bonds specified in brackets.

	$Pa\bar{3}$	$Cmca(1)$	$Cmca(2)$	$P2_12_12_1$	$I\bar{4}2d$	$P4_2/mnm$
a	5.283	5.075	4.561	7.024	3.888	3.789
b	5.283	4.553	5.128	3.922	3.888	3.789
c	5.283	6.400	6.337	6.665	5.896	2.429
Z	4	4	4	8	4	2
V_0	36.87	36.97	37.05	22.95	22.28	17.44
B_0	16.6	15.0		133.6	142.7	327.2
$d_{C–O}$	1.168(2)	1.168(2)	1.265(2)	1.385(4)	1.385(4)	1.577(4)
						1.679(2)
$d^{nn}_{C–O}$	2.863(6)	2.841(2T)	2.814(4P)			
		2.959(4P)	2.900(2T)			
$d_{O–O}$	2.336(1)	2.337(1)	2.529(1)	2.190(1)	2.219(4)	2.008(1)
	2.941(6)	2.941(5)	2.909(6)	2.244(3)	2.362(2)	2.303(8)

Table 2. Topological characteristics of the bond critical points as obtained in the AIM analysis of the crystal structures here considered. We have found several intra- and inter-molecular bond critical points with different multiplicities (in parentheses). r_1 and r_2 stand for the linear distances from the bond critical point to the first and second atom of the bond pair, respectively, α being the average angle involved in the bond path. T and P designate, respectively, the T-like and parallel configurations of two CO_2 units in the molecular CO_2-III phase. All data in atomic units.

	Bond	ρ_b	$\nabla^2\rho_b$	r_1/r_2	α (deg)	Remarks
$Pa\bar{3}$	C–O(8)	0.4523	0.9395	0.5042	180	Intramolecular
	O–O(24)	0.0219	0.0969	1.1579	146	Intermolecular
$Cmca(1)$	C–O(8)	0.4452	0.8704	0.5030	180	Intramolecular
	O–O(28)	0.0201	0.0090	1.0429		Intermolecular (P, T)
$Cmca(2)$	C–O(8)	0.3816	0.0980	0.4986	180	Intramolecular
	C–O(8)	0.0177	0.0763	1.0088	172	Intermolecular (T)
	O–O(36)	0.0240	0.1125	0.9867		Intermolecular (P, T)
$P2_12_12_1$	C–O(32)	0.2878	−0.7520	0.5530	176	
	O–O(28)	0.0177	0.0619	0.9891	178	
$I\bar{4}2d$	C–O (16)	0.2896	−0.7506	0.5479	176	
	O–O(16)	0.0154	0.0545	0.9831	178	
$P4_2/mnm$	C–O(8)	0.1944	−0.1735	0.7203	180	
	C–O(4)	0.1456	0.0392	0.7611	180	
	O–O(4)	0.0157	0.0622	1.0000	180	

3.2. Chemical bonding

Table 2 gathers the results of our AIM topological analysis. Let us first examine the evolution of the intra-molecular C–O bonds. We can easily distinguish three different regimes. Both the cubic and the $Cmca(1)$ phases share a basically isolated molecule with a large density and a large, positive Laplacian, at the bond critical point. This is the known behaviour of the polar C–O bond in CO_2. In a similar way, the $P2_12_12_1$ and $I\bar{4}2d$ polymeric phases display a completely different intra-molecular critical point. The value of ρ_b is roughly two thirds that in the isolated molecule, and the C–O interatomic surface has crossed the zero

Table 3. Calculated atomic charges, volumes, bulk moduli, and occupation factors (f_i) of CO_2 polymorphs according to the AIM analysis.

	Atom	$\mathcal{Q}_i$ (e)	V_i (bohr^3)	B_i (GPa)	f_i
$Pa\bar{3}$	C	2.31	28.8	23.2	0.116
$B_0 = 16.6$	O	−1.15	109.4	17.0	0.884
$Cmca(1)$	C	2.29	29.7	17.0	0.121
$B_0 = 15.0$	O	−1.15	106.9	14.7	0.879
$Cmca(2)$	C	1.96	40.4		0.163
	O	−0.98	103.8		0.837
$I\bar{4}2d$	C	2.04	18.9	101.3	0.126
$B_0 = 142.7$	O	−1.03	65.7	156.1	0.874
$P4_2/mnm$	C	1.44	22.5	206.9	0.192
$B_0 = 327.2$	O	−0.72	47.5	389.0	0.808

Laplacian isosurface, becoming negative. This is typical of a C–O single bond, and marks a complete polymerization. For instance, in methanol, a 6-311 + $G(p, d)$ Hartree–Fock [30] calculation gives $d_{C–O} = 1.404$ Å, $\rho_b = 0.2566$ au. More interesting are the rest of the cases. First, the $P4_2/mnm$ phase displays a very peculiar C–O bond, with a very small density and positive Laplacian, and what is more interesting, a very unusual r_1/r_2 ratio, signalling a too large carbon and a very weak link to its six neighbouring oxygens. This is probably not a stable arrangement at the considered compression rates. On the other hand, the C–O intramolecular bond in the hypothetical $Cmca(2)$ structure is particularly interesting, for it is clearly intermediate, between the molecular and polymeric phases. All topological indices point towards a soft weakening of this intramolecular bond due to interactions with other molecules of the environment.

The C–O intermolecular bonds that appear in the $Cmca(2)$ structure substitute some of the O–O bond critical points of the $Cmca(1)$ phase. This is accompanied by a clearly visible decrease of the quadrupole atomic moment of carbon, in such a way that the bond path now connects carbon and oxygen, and not oxygen and oxygen. In its turn, this generates four-fold planar coordinated carbons. It is also to be noticed that this inter-molecular C–O bond paths are rather curved (see α in table 2). This has usually [18] been associated to bond stress or to the presence of nearby electronic instabilities. One may easily imagine a distortion of these stressed bonds in which the inter-molecular C–O distance decreases as two C–O bonds execute an out-of-plane movement that generates a tetrahedral-like coordination. Such distortions of this structure need much further study.

3.3. Atomic equations of state

The evaluation of the atomic volumes at different pressures provides equations of state for C and O in all the phases explored. Regardless of pressure and crystalline structure, oxygen occupies more than 80% of the unit cell volume, and, therefore, a similar trend of the oxygen and crystal bulk moduli along the phases studied should be expected. This result can be observed in table 3 and is in concordance with the AIM analysis in oxide spinels [31] and anatase TiO_2 [32]. Since the atomic volumes fill up the unit cell space, the macroscopic compressibility (κ) can be decomposed in atomic contributions (κ_i) using the following expression [31]:

$$\kappa = \frac{1}{B} = \sum_i f_i \kappa_i, \qquad f_i = \frac{n_i V_i}{V}, \qquad \kappa_i = -\frac{1}{V_i}\frac{\partial V_i}{\partial p}, \tag{1}$$

where i runs over the non-equivalent atoms in the unit cell, and n_i is the number of equivalent atoms i in the unit cell. This simple partition is very useful because the local compressibilities can be transferred to different materials.

We find a distinctive behaviour between molecular and non-molecular phases. The former has higher B_C values due to the localization of the C electron density between the two O atoms of the CO_2 molecular unit. In the polymeric structures, lower compressibilities are obtained for both atoms, though O atoms now exhibit higher B_i values (see table 3). This result contrasts with that obtained in oxide spinels and anatase TiO_2 and illustrates a non-ionic character of these polymeric CO_2 structures. It is to be emphasized that the O behaviour resembles that of N in the hard nitride spinels of group-IV [33], suggesting a potential low compressibility for CO_2-V polymorphs which is only obtained for the stishovite structure according to the present calculations.

4. Conclusions

Total energy calculations with structural optimizations and microscopic topological analysis of electron densities have been performed in CO_2 polymorphs using first-principles techniques. Clear trends in the interatomic distances, equilibrium volumes, and zero pressure bulk moduli illustrate the progressive transformation of solid CO_2 from a molecular to a polymeric crystalline lattice. A similar image is obtained from the C–O bonding analysis: high ρ_b and positive $\nabla^2\rho_b$ values in CO_2-I and CO_2-III contrast with lower ρ_b and negative $\nabla^2\rho_b$ values in CO_2-V polymorphs. A hypothetical $Cmca$ CO_2-III structure is proposed as a precursor for a four-fold carbon coordinated phase. This result is clearly supported by the existence of bond critical points connecting CO_2 molecules associated in a T-like configuration. The bulk compressibility decomposition discriminates the molecular solids (with C being less compressible than O) from the polymeric structures that do not exhibit super-hard atomic properties except in the highly strained hypothetical stishovite lattice. We believe that these results can provide useful information for further investigations of the mechanistic aspects of the transition from CO_2-III to a bent-like CO_2-IV phase [14].

Acknowledgments

Financial support from Spanish DGICYT (Projects BQU2000-0466, BQU2003-06553 and BQU2000-1425) and Fundació Bancaixa (Project P1-IA2002-05) is acknowledged. L Gracia and M Marqués thank the Spanish MCYT for graduate grants.

References

[1] Kuchta B and Etters R D 1993 *Phys. Rev.* B **47** 14691
[2] Aoki K, Yamawaki H and Sakashita M 1993 *Phys. Rev.* B **48** 9231
[3] Aoki K, Yamawaki H, Sakashita M, Gotoh Y and Takemura K 1994 *Science* **263** 356
[4] Lu R and Hofmeister A M 1995 *Phys. Rev.* B **52** 3985
[5] Olijnyk H and Jephcoat A P 1998 *Phys. Rev.* B **57** 879
[6] Gygi F 1998 *Comput. Mater. Sci.* **10** 63
[7] Iota V, Yoo C S and Cynn H 1999 *Science* **283** 1510
[8] Serra S, Cavazzoni C, Chiarotti G L, Scandolo S and Tosatti E 1999 *Science* **284** 788
[9] Yoo C S, Cynn H, Gygi F, Galli G, Iota V, Nicol M, Carlson S, Hausermann D and Mailhiot M 1999 *Phys. Rev. Lett.* **83** 5527
[10] Dong J, Tomfohr J K and Sankey O F 2000 *Science* **287** 11a
[11] Dong J, Tomfohr J K and Sankey O F 2000 *Phys. Rev.* B **61** 5967

[12] Dong J, Tomfohr J K, Sankey O F, Leinenweber K, Somayazulu M and McMillan P F 2000 *Phys. Rev.* B **62** 14685
[13] Holm B, Ahuja R, Belonoshko A and Johansson B 2000 *Phys. Rev. Lett.* **85** 1258
[14] Iota V and Yoo C S 2001 *Phys. Rev. Lett.* **86** 5922
[15] Yoo C S, Iota V and Cynn H 2001 *Phys. Rev. Lett.* **86** 444
[16] Yoo C S, Kohlmann H, Cynn H, Nicol M F, Iota V and LeBihan T 2002 *Phys. Rev.* B **65** 104103
[17] Tschauner O, Mao H and Hemley R J 2001 *Phys. Rev. Lett.* **87** 075701
[18] Bader R F W 1990 *Atoms in Molecules* (Oxford: Oxford University Press)
[19] Martín Pendás A, Costales A and Luaña V 1998 *J. Phys. Chem.* B **102** 6937
[20] Kresse G and Furthmuller J 1996 *Phys. Rev.* B **54** 11169
[21] Ceperley D M and Alder B J 1980 *Phys. Rev. Lett.* **45** 566
[22] Kresse G and Joubert J 1999 *Phys. Rev.* B **59** 1758
[23] Blanco M A, Francisco E and Recio J M 1992 *The* `GIBBS` *code* (miguel@carbono.quimica.uniovi.es)
[24] Francisco E, Recio J M, Blanco M A, Martín Pendás A and Costales A 1998 *J. Phys. Chem.* A **102** 1595
[25] Saunders V R, Dovesi R, Roetti C, Causá M, Harrison N M, Orlando R and Zicovich-Wilson C M 1998 *CRYSTAL98 User's Manual* (Torino: University of Torino)
[26] Martín Pendás A and Luaña V 1995 *The* `CRITIC` *code* (angel@fluor.quimica.uniovi.es)
[27] Olinger B 1982 *J. Chem. Phys.* **77** 6255
[28] Liu L 1984 *Earth Planet. Sci. Lett.* **71** 104
[29] Hanson R C 1985 *J. Phys. Chem.* **89** 4499
[30] Gaussian, Inc. 1998 *Gaussian 98* (Pittsburgh, PA: Gaussian)
[31] Martín Pendás A, Costales A, Blanco M A, Recio J M and Luaña V 2000 *Phys. Rev.* B **62** 13970
[32] Calatayud M, Mori-Sánchez P, Beltrán A, Martín Pendás A, Francisco E, Andrés J and Recio J M 2001 *Phys. Rev.* B **64** 184141
[33] Mori-Sánchez P, Marqués M, Beltrán A, Jiang J Z, Gerward L and Recio J M 2003 *Phys. Rev.* B **68** 064115